THE JOURNAL OF BIOLOGICAL CHEMISTRY
Vol. 276, No. 44, Issue of November 2, pp. 41005–41013, 2001
Printed in U.S.A.

Calcium-regulated DNA Binding and Oligomerization of the Neuronal Calcium-sensing Protein, Calsenilin/DREAM/KChIP3*

Received for publication, June 22, 2001, and in revised form, August 22, 2001
Published, JBC Papers in Press, September 4, 2001, DOI 10.1074/jbc.M105842200

Masanori Osawa‡, Kit I. Tong§, Christina Lilliehook¶, Wilma Wasco‖, Joseph D. Buxbaum¶, H.-Y. Mary Cheng, Josef M. Penninger**, Mitsuhiko Ikura§, and James B. Ames‡ ‡‡**

*From the ‡Center for Advanced Research in Biotechnology, University of Maryland Biotechnology Institute, Rockville, Maryland 20850, §Division of Molecular and Structural Biology, Ontario Cancer Institute and Department of Medical Biophysics, University of Toronto, Toronto, Ontario M5G 2M9, Canada, ¶Departments of Psychiatry and Neurobiology, Mount Sinai School of Medicine, New York, New York 10029, ‖Department of Neurology, Massachusetts General Hospital, Harvard Medical School, Charlestown, Massachusetts 02129, and **Amgen Institute, Ontario Cancer Institute, and the Departments of Medical Biophysics and Immunology, University of Toronto, Toronto, Ontario M5G 2C1, Canada*

Calsenilin/DREAM/KChIP3, a member of the recoverin branch of the EF-hand superfamily, interacts with presenilins, serves as a calcium-regulated transcriptional repressor, and interacts with A-type potassium channels. Here we report physicochemical characterization of calcium binding, oligomerization, and DNA binding of human calsenilin/DREAM/KChIP3. Equilibrium Ca^{2+} binding measurements indicate that the protein binds 3 Ca^{2+} with a dissociation constant of 14 μM and a Hill coefficient of 0.7. Dynamic light scattering and size exclusion chromatography show that the Ca^{2+}-bound protein exists as a dimer at protein concentrations lower than 150 μM and forms a tetramer at concentrations above 200 μM. The Ca^{2+}-free protein is a tetramer in the concentration range 20–450 μM. Isothermal titration calorimetry and dynamic light scattering indicate that the Ca^{2+}-free protein tetramer binds endothermically (ΔH = +25 kcal/mol) to four molecules of DNA derived from the downstream regulatory element (DRE) of either the prodynorphin or c-*fos* genes. One DRE molecule binds tightly to the protein with a dissociation constant (K_d) of 75 nM, and the other three bind more weakly (K_d = 640 nM). No significant DNA binding was observed for the Ca^{2+}-bound protein. The N-terminal protein fragment (residues 1–70) binds nonspecifically to DRE in a Ca^{2+}-independent manner, whereas a C-terminal fragment containing the four EF-hands (residues 65–256) binds DRE (K_d = 200 nM) in a Ca^{2+}-regulated and sequence-specific fashion. The C-terminal fragment is a tetramer in the Ca^{2+}-free state and dissociates into dimers at saturating Ca^{2+} levels.

Calcium ion (Ca^{2+}) regulates many important physiological processes including gene expression, neuronal synaptic plasticity, and cell death (1). The effects of changes in intracellular Ca^{2+} levels are mediated primarily by Ca^{2+}-binding proteins that belong to the EF-hand superfamily (2, 3). The recoverin subgroup includes neuronal calcium sensors such as recoverin (4), neurocalcin (5), and frequenin (6), all of which are *N*-myristoylated and possess four EF-hand motifs (7) (Fig. 1). A characteristic feature of the recoverin family is the sequence CP*X*G that prevents the binding of Ca^{2+} to the first EF-hand. Recently, a new member of the recoverin family variously named calsenilin (8), DREAM[1] (9), and KChIP3 (10) has been identified in the human brain and reported to have several biological functions.

Calsenilin was first identified by the yeast two-hybrid system to interact with the C-terminal 40 residues of presenilin 2, a membrane protein genetically linked to Alzheimer's disease (8). Calsenilin consists of 256 amino acids, and the C-terminal 190 residues are about 40% identical in amino acid sequence to frequenin, a representative protein of the recoverin family (Fig. 1). Recently, it has been reported that calsenilin reverses the presenilin-mediated enhancement of Ca^{2+} signaling (11) and that calsenilin is a substrate for caspase-3 that also interacts with the C-terminal region of presenilin 2 (12).

The protein named DREAM was reported as the first Ca^{2+}-regulated transcriptional repressor (9). DREAM represses the transcription of human prodynorphin and c-*fos* genes in the brain by binding to the DRE only in the absence of calcium and derepresses the transcription at high Ca^{2+} levels. DREAM also binds to a silencer sequence in the 3′-untranslated region of the apoptotic gene *hrk* and represses the expression of downstream reporter genes (13). The human DREAM protein was originally reported to consist of 284 residues (9), in which the C-terminal 256 residues are identical to calsenilin. A more recent study has revealed that the C-terminal 256 residues of DREAM are sufficient for the calcium-regulated transcriptional repression (14, 15). However, the precise length of the endogenous DREAM protein (284 *versus* 256 residues) is still not known, and it is still unclear how DREAM recognizes the different DRE sequences of prodynorphin and c-*fos*.

The potassium channel-interacting proteins KChIP1 and KChIP2 were identified by the yeast two-hybrid system to interact with the N-terminal 180 residues of A-type voltage-gated potassium (Kv4.2) channels (10). KChIP1 and KChIP2

* This work was supported in part by National Institutes of Health Grants EY12347 (to J. B. A.) and AG15801 and AG05138 (to J. D. B.) and by a Human Frontier Science Program long-term postdoctoral fellowship (to M. O.). The costs of publication of this article were defrayed in part by the payment of page charges. This article must therefore be hereby marked "*advertisement*" in accordance with 18 U.S.C. Section 1734 solely to indicate this fact.

‡‡ Recipient of the Arnold and Mabel Beckman Foundation Young Investigator Award. To whom correspondence should be addressed: Center for Advanced Research in Biotechnology, University of Maryland Biotechnology Institute, 9600 Gudelsky Dr., Rockville, MD 20850. Tel.: 301-738-6120; Fax: 301-738-6255; E-mail: james@carb.nist.gov.

[1] The abbreviations used are: DREAM, downstream regulatory element antagonist modulator; apo-DREAM, Ca^{2+}-unbound DREAM; Ca^{2+}-DREAM, Ca^{2+}-bound DREAM; mDREAM, mouse DREAM; DRE, downstream regulatory element; DynDRE, prodynorphin DRE; DLS, dynamic light scattering; ITC, isothermal titration calorimetry; EMSA, electrophoretic mobility shift analysis; LDAO, lauryldimethylamine oxide; DTT, dithiothreitol.

also bind to intact Kv4.2 channels and activate channel kinetics only at high Ca^{2+} levels. Notably, the N-terminal 70 residues of KChIP1 and KChIP2 do not contribute significantly to the modulation of Kv4.2 channels. Interestingly, KChIP1 and KChIP2 are more than 70% identical in sequence to calsenilin (Fig. 1), and calsenilin was also shown to interact with Kv4.2 channels. Hence, calsenilin is also referred to as KChIP3.

The single protein variously named calsenilin, DREAM, and KChIP3 appears to possess multiple functions in different compartments of the cell by regulating completely different target molecules. Calsenilin binds and regulates presenilin proteins in the endoplasmic reticulum, calcium-free DREAM binds to DRE sequences of DNA in the cell nucleus, and calcium-bound KChIP3 may bind and activate Kv4.2 channels on the plasma membrane. Therefore, it is of particular interest to learn how this one protein can bind and recognize several different target molecules. Here we report the physicochemical characterization of the multifunctional protein calsenilin/DREAM/KChIP3 (referred to hereafter as DREAM) as an important step toward understanding its various mechanisms of target recognition. Furthermore, we have characterized the novel DNA binding properties of this protein, and we suggest a possible mechanism for Ca^{2+}-regulated gene expression.

EXPERIMENTAL PROCEDURES

Expression and Purification of Human Calsenilin/DREAM/KChIP3—The coding sequence of human calsenilin/DREAM/KChIP3 was amplified by polymerase chain reaction from a mammalian expression vector (pcDNA3.1) containing calsenilin/DREAM cDNA using the primers 5′-CTAGGCCTCATATGCAGCCGGCTAAGGAAG-3′ and 5′-CTAGGCCTCTCGAGGATGACATTCTCAAAC-3′. The resulting product was ligated into pET-22b(+) (Novagen) using the sites for *Nde*I and *Xho*I. The sequence was verified by sequencing.

After the transformation of the construct into *Escherichia coli* BL21 (DE3) (Stratagene), the calsenilin/DREAM/KChIP3 protein with a 6×His tag at the C terminus was overexpressed as inclusion bodies. Strains were grown in 2 liters of LB media with 100 μg/ml ampicillin at 37 °C. When the optical density of the culture at 600 nm had reached 0.8, isopropyl-1-thio-β-D-galactopyranoside was added to the culture to a final concentration of 0.7 mM, and the culture was further incubated for 3.5 h at 37 °C. Cells were harvested by centrifugation, resuspended in lysis buffer (20 mM Tris-HCl, pH 8.0, 0.1 M KCl, 10% (v/v) glycerol, 1 mM β-mercaptoethanol, and 0.1 mM phenylmethylsulfonyl fluoride), and disrupted by French press at 900 p.s.i. Disruption by French press was repeated once. Cell debris and inclusion bodies were collected by centrifugation. The pellet was suspended in wash buffer (1.0% (v/v) Triton X-100 in the lysis buffer), homogenized, and sonicated, and the insoluble material was collected by centrifugation. This wash was repeated three times. The pellet from the last wash was suspended in guanidine buffer (6 M guanidine-HCl, 0.1 M sodium phosphate, 10 mM Tris-HCl, pH 8.0, and 1 mM β-mercaptoethanol), homogenized, and incubated for 15 min at room temperature. After centrifugation to remove insoluble material, the supernatant was applied onto a Talon (CLONTECH) column previously equilibrated in the guanidine buffer. After washing the column with the guanidine buffer, the protein was eluted with imidazole buffer (0.1 M imidazole in the guanidine buffer). The eluted solution was dialyzed *versus* refolding buffer (10 mM Tris-HCl, pH 7.4, 0.3 M NaCl, 10% (v/v) glycerol, 0.1 M EDTA, and 1 mM DTT) for 24 h. Then, 10 mM lauryldimethylamine oxide (LDAO) was added to the sample, which was dialyzed *versus* LDAO buffer (10 mM Tris-HCl, pH 7.4, 10 mM LDAO, 1 mM EDTA, and 1 mM DTT). The sample was applied onto a DEAE column previously equilibrated in the LDAO buffer, and then it was eluted with NaCl gradient (0–0.3 M NaCl over 3 h at 2 ml/min). Further purification of DREAM was achieved using a size exclusion column (S-300 HR) with the LDAO buffer.

Expression and Purification of Mouse DREAM and Deletion Mutants—Genes encoding mouse DREAM and its deletion mutants (residues 1–70, mut1–70; residues 1–96, mut1–96; residues 65–256, mut65–256) were inserted into pET15b (Novagen) expression vectors. These constructs were transformed into *E. coli* BL21 (DE3) (Stratagene) cells and grown in 2 liters of LB media with 100 μg/ml ampicillin at 37 °C. After the induction with 0.7 mM isopropyl-1-thio-β-D-galactopyranoside, cultures were incubated for another 3 h. Cells were harvested by centrifugation and resuspended in buffer A (20 mM Tris-HCl, pH 8.0, 20% (v/v) glycerol, 0.3 M NaCl, and 1 mM phenylmethylsulfonyl fluoride) containing 10 mM β-mercaptoethanol, 0.2% Tween 20, 20 μg/ml DNase I, 5 mM $MgCl_2$, and 30 mg of lysozyme. Cell suspensions were incubated at 4 °C for 1.5 h and then sonicated (Branson's Sonifier 450) on ice twice for 3 min at setting 10 with 10% duty cycle. Soluble protein fractions were recovered by centrifugation and loaded onto Talon (CLONTECH) beads previously equilibrated with buffer A. After washing with buffer A containing 15 mM imidazole, proteins were eluted with buffer A containing 0.15 M imidazole. The mut1–96 and mut65–256 samples were further purified for ITC experiments with DEAE column in the same way as human DREAM.

Preparation of Synthetic Oligonucleotides—Oligonucleotides used in this study represent DRE of human prodynorphin (DynDRE) and c-*fos* (c-*fos* DRE): DynDRE-1, 5′-GAAGCCGGAGTCAAGGAGGCCCCTG-3′; DynDRE-2, 5′-CAGGGGCCTCCTTGACTCCGGCTTC-3′; c-*fos* DRE-1, 5′-CTGCAGCGAGCAACTGAGAATCCAAGAC-3′; and c-*fos* DRE-2, 5′-GTCTTGGATTCTCAGTTGCTCGCTGCAG-3′. For ITC and dynamic light scattering (DLS) experiments, 10 μmol of each oligonucleotide was synthesized on a DNA synthesizer by the solid phase phosphoramidate method and purified by fast protein liquid chromatography on a Zorbax oligonucleotide column (DuPont) using the volatile buffer containing 32 mM NaH_2PO_4 (pH 7.0) and 20% (v/v) acetonitrile with an NaCl gradient. After lyophilization of the eluted fractions, the sample was dissolved with 2 ml of H_2O and desalted using a PD-10 gel filtration column (Amersham Pharmacia Biotech). Desalted DNA was precipitated using EtOH/sodium acetate followed by evaporation of the solvent. Cy5 (Amersham Pharmacia Biotech) 5′-labeled oligonucleotides used for fluorescent EMSA were purchased from ACGT Corp. (Toronto, Canada). The same sequences of DynDRE-1 and DynDRE-2 mentioned above were used. For competition experiments, unlabeled double-stranded oligonucleotides of DynDRE, the canonical AP-1 from the collagenase gene (cAP-1), 5′-AAGCTTGCATGACTCAGACAG-3′, and mutated unlabeled double-stranded oligonucleotides of human DynDRE (DREmut5, 5′-GAAGCCGGA**A**TCAAGGAGGCCCCTG-3′; DREmut4, 5′-GAAGCCGGA**AA**CAAGGAGGCCCCTG-3′; mutation shown in bold) were used as unlabeled competitors (16). Complementary strands were dissolved in annealing buffer (10 mM Tris-HCl, pH 7.4), completely denatured at 95 °C, and annealed by slowly cooling to room temperature. Formation of double-stranded DNA was checked on a 20% nondenaturing polyacrylamide/0.25× Tris-borate EDTA/1% (v/v) glycerol gel before binding reactions. The concentrations were determined via UV spectrometry.

Binding of $^{45}Ca^{2+}$—The binding of $^{45}Ca^{2+}$ to DREAM was measured as the protein-bound radioactivity retained after ultrafiltration using a procedure described previously (17). Briefly, DREAM (20 μM) in 1.6 ml of 20 mM Tris (pH 7.4), 10 mM LDAO, and 1 mM DTT was placed in the sample compartment of a Centricon-10 concentrator (Millipore), and 20 μl of 0.25 mM $^{45}CaCl_2$ (1 μCi) was added as a radioactive tracer. The sample was subjected to centrifugation (at 2000 rpm) in a tabletop centrifuge (Beckman model TJ-6) at room temperature for 30 s, forming 20 μl of filtrate. The radioactivity in the filtrate (free Ca^{2+}) and the radioactivity in an equal volume of the protein sample (total Ca^{2+}) were determined by liquid scintillation counting. Successive additions of nonradioactive Ca^{2+} were made to the protein sample, and the above-mentioned procedure was repeated. After each addition of nonradioactive ligand, the free Ca^{2+} concentration was calculated from the measured radioactivity as follows:

$$Ca^{2+}_{free} = \frac{r_a}{r_b} Ca^{2+}_{total} \quad \text{(Eq. 1)}$$

where r_a is the measured radioactivity of the filtrate, r_b is radioactivity of protein sample, and Ca^{2+}_{total} is the total Ca^{2+} concentration. The concentration of Ca^{2+} bound to protein is therefore

$$Ca^{2+}_{bound} = Ca^{2+}_{total} - Ca^{2+}_{free} \quad \text{(Eq. 2)}$$

Spectroscopic Analyses—Structural differences between the apo- and Ca^{2+}-loaded form of DREAM and mut65–256 were investigated by CD spectroscopy and fluorescence spectroscopy. The protein concentration was 5–10 μM dissolved in 10 mM Tris-HCl, pH 7.4, 1 mM DTT, and 1 mM EDTA for apo-DREAM. After the measurement for the apo-protein, the small amount of 1 M $CaCl_2$ solution was injected to the sample, giving a final Ca^{2+} concentration of 5 mM for the Ca^{2+}-loaded form. CD spectra were measured on a J-720 CD spectropolarimeter (JASCO) at 25 °C. A cell path length of 1 mm was used. Each spectrum was collected with eight scans spanning wavelengths from 195 to 250 nm. Fluorescence spectra were recorded on a FluoroMax-2 fluorometer (Instruments S.A., Inc.). Excitation and emission were at 295 and 310–440 nm, respectively.

```
                          1        10        20        30        40        50
h-calsenilin/DREAM        MQPAKEVTKA SDGSLLGDLG HTPLSKKEGI KWQRPRLSRQ ALMRCCLVKW
m-calsenilin/DREAM        MQRTKEAVKA SDGSLLGDPG RIPLSKRESI KWQRPRFTRQ ALMRCCLIKW
frequenin                 .......... .......... .......... .......... ..........
neurocalcin               .......... .......... .......... .......... ..........
recoverin                 .......... .......... .......... .......... ..........

                                  60        70        80        90       100
h-calsenilin/DREAM        ILSSTAPQGS DSSDSELELS TVRHQPEGLD QLQAQTKFTK KELQSLYRGF
m-calsenilin/DREAM        ILSSAAPQGS DSSDSELELS TVRHQPEGLD QLQAQTKFTK KELQSLYRGF
frequenin                 .......... .....MG.KK SSKLKQDTID RLTTDTYFTE KEIRQWHKGF
neurocalcin               .......... .....MG.KQ NSKLRPEVMQ DLLESTDFTE HEIQEWYKGF
recoverin                 .......... .....MGNSK SGALSKEILE ELQLNTKFTE EELSSWYQSF

                                 110       120       130       140       150
h-calsenilin/DREAM        KNECPTGLVD EDTFKLIYAQ FFPQGDATTY AHFLFNAFDA DGNGAIHFED
m-calsenilin/DREAM        KNECPTGLVD EDTFKLIYSQ FFPQGDATTY AHFLFNAFDA DGNGAIHFED
frequenin                 LKDCPNGLLT EQGFIKIYKQ FFPQGDPSKF ASLVFRVFDE NNDGSIEFEE
neurocalcin               LRDCPSGHLS MEEFKKIYGN FFPYGDASKF AEHVFRTFDA NGDGTIDFRE
recoverin                 LKECPSGRIT RQEFQTIYSK FFPEADPKAY AQHVFRSFDA NSDGTLDFKE

                                 160       170       180       190       200
h-calsenilin/DREAM        FVVGLSILLR GTVHEKLKWA FNLYDINKDG YITKEEMLAI MKSIYDMMGR
m-calsenilin/DREAM        FVVGLSILLR GTVHEKLKWA FNLYDINKDG CITKEEMLAI MKSIYDMMGR
frequenin                 FIRALSVTSK GNLDEKLQWA FRLYDVDNDG YITREEMYNI VDAIYQMVG-
neurocalcin               FIIALSVTSR GKLEQKLKWA FSMYDLDGNG YISKAEMLEI VQAIYKMVS-
recoverin                 YVIALHMTSA GKTNQKLEWA FSLYDVDGNG TISKNEVLEI VTAIFKMISP

                                 210       220       230       240       250
h-calsenilin/DREAM        HTYPILRED- -APAEHVERF FEKMDRNQDG VVTIEEFLEA CQKDENIMSS
m-calsenilin/DREAM        HTYPILRED- -APLEHVERF FQKMDRNQDG VVTIDEFLET CQKDENIMNS
frequenin                 -Q-QPQSEDE NTPQKRVDKI FDQMDKNHDG KLTLEEFREG SKADPRIVQA
neurocalcin               -SVMKMPEDE STPEKRTEKI FRQMDTNRDG KLSLEEFIRG AKSDPSIVRL
recoverin                 EDTKHLPEDE NTPEKRAEKI WGFFGKKDDD KLTEKEFIEG TLANKEILRL

h-calsenilin/DREAM        MQLFENVI  256
m-calsenilin/DREAM        MQLFENVI  256
frequenin                 LSLGGG  187
neurocalcin               LQCDPSSAGQ F  193
recoverin                 IQFEPQKVKE KLKEKKL  202
```

FIG. 1. **Alignment of the amino acid sequence of human and mouse calsenilin/DREAM with various members of the recoverin branch of the EF-hand superfamily.** The Ca^{2+}-binding loops of the four EF-hands are *underlined*. Residues highlighted in *bold* in EF-1 prevent Ca^{2+} binding.

DLS—The molecular mass of DREAM was examined by DLS using DynaPro-MS (Protein Solutions) at 25 °C. First, screening for a good condition to give a monomodal distribution was carried out using 30–50 μM DREAM in various buffers. 0.1 ml of each sample was centrifuged at 15,000 rpm for 30 min and passed through a filtering assembly containing a 0.1 μm filter into a 12-μl chamber quartz cuvette. At least 15 measurements were repeated. The data were analyzed using Dynamics 4.0 and DynaLS software as described by Moradian-Oldak *et al.* (18). The samples for the experiments examining concentration dependence of the molecular mass were prepared by dilution of the protein stock solutions previously dialyzed against 10 mM Tris-HCl, pH 7.4, 10 mM LDAO, 1 mM DTT, and 1 mM EDTA or 5 mM $CaCl_2$ for apo- and Ca^{2+}-DREAM, respectively. The samples diluted with the dialysis buffer were incubated overnight at 4 °C before the DLS experiments.

Size Exclusion Chromatography—Determination of the molecular mass of the purified DREAM and mut65–256 in the Ca^{2+}-bound and unbound form in solution was carried out on a Superdex 200 HR 10/30 column (Amersham Pharmacia Biotech) at 4 °C in the buffers containing 20 mM Tris-HCl, pH 7.4, 10 mM LDAO, 1 mM DTT, and 5 mM $CaCl_2$ for Ca^{2+}-DREAM or 1 mM EDTA for apo-DREAM. Separate aliquots (0.1 ml) of DREAM (8.7 and 87 μM) and mut65–256 (87 μM) were loaded onto the column and eluted at a flow rate of 0.4 ml/min. Apparent molecular masses were calculated using a standard curve of V_e/V_0 *versus* the log of the molecular masses of standard proteins (β-amylase, 200 kDa; alcohol dehydrogenase, 150 kDa; transferrin, 81 kDa; carbonic anhydrase, 29 kDa; and myoglobin, 17 kDa). V_0 is a void volume obtained using blue dextran (2000 kDa), and V_e is a volume of elution.

ITC—Binding of DREAM to DynDRE and c-*fos* DRE was measured by ITC (19) using a MicroCal VP-ITC MicroCalorimeter (MicroCal Inc.). The protein and DNA samples were dialyzed against a buffer containing 10 mM Tris-HCl, pH 7.4, 10 mM LDAO, 1 mM DTT, and 5 mM $CaCl_2$ or 1 mM EDTA for the Ca^{2+}-bound and unbound form, respectively. Experiments were performed at 35 °C. A stock solution of DREAM (525–560 μM) was titrated by injection of a total of 290 μl of 15–25 μM DNA in 29 aliquots. Heats of dilution were determined by titrating DREAM into the dialysis buffer and subtracted from the raw titration data before data analysis using MicroCal Origin version 5.0 provided by the manufacturer. Because the observed binding isotherm appeared multiphasic, the data were analyzed using a two-site binding model, resulting in the best fit of thermodynamic parameters to the titration. Binding of mut1–96 and mut65–256 to DynDRE was also measured in the same way.

Fluorescent EMSA—Proteins were exchanged firstly to 20 mM Tris-HCl, pH 7.4, 10% (v/v) glycerol, 100 mM NaCl, 5 mM DTT, and 0.5 mM EDTA using PD-10 columns and concentrated to 115 μM (mut1–70), 330 μM (mut65–256), and 80 μM (full length) by Centricon 3 or 10 (Millipore) at 4 °C. Proteins were then incubated with 5 nM Cy5-labeled DNA for 5 h at room temperature in 10 mM HEPES, pH 7.9, 8 mM $MgCl_2$, 0.1 mM EDTA, 2 mM DTT, and 0.005 unit/ml poly(dI-dC) (Amersham Pharmacia Biotech) with or without 10 mM $CaCl_2$. Protein·DNA complexes were resolved in 5% nondenaturing polyacrylamide/0.25× Tris-borate EDTA/1% (v/v) glycerol gels at 200 V for 30 min in 0.25× Tris-borate EDTA and 0.5 mM $MgCl_2$ running buffer. Wet fluorescent gels were scanned using red fluorescence mode of a Storm 860 system (Molecular Dynamics) with a voltage setting of 1000 V and a scanning resolution of 200 μm. For DNA competition experiments, a 15-fold excess of unlabeled double-stranded competitive oligonucleotides was added to competition assays of wild type or mut65–256, and a 65-fold excess of unlabeled DNA was added to the competition assays of mut1–70 1 h before further incubation with the labeled oligonucleotides.

RESULTS AND DISCUSSION

Ca^{2+} Binding Studies—DREAM contains an N-terminal basic region (residues 1–65) and a C-terminal Ca^{2+}-binding region (residues 70–256) containing four EF-hand motifs that are similar in sequence to the Ca^{2+}-binding sites found in calmod-

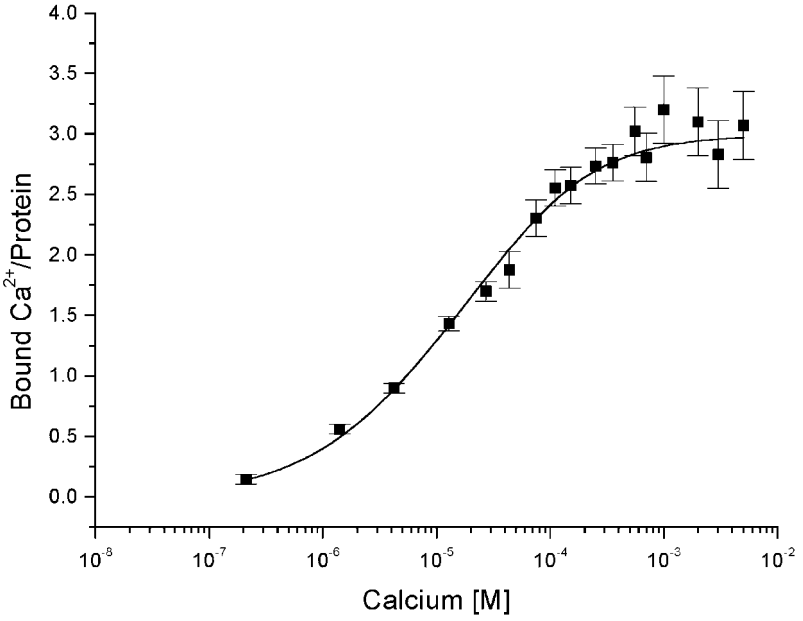

FIG. 2. **Equilibrium Ca^{2+} binding to DREAM.** Titration of $^{45}Ca^{2+}$ binding to DREAM was conducted using an ultrafiltration method as described under "Experimental Procedures." The number of ions bound/protein is plotted *versus* the free calcium concentration. The *error bars* were estimated as the standard deviation of three measurements. The *solid line* represents the best fit to the Hill model using a dissociation constant of 14 μM and a Hill coefficient of 0.7.

ulin, troponin C, and recoverin. Like other members of the recoverin family (Fig. 1), the first EF-hand from the N terminus (EF-1) of DREAM contains substitutions (Cys-104 and Pro-105) that are expected to disrupt the structure of this binding loop and prevent Ca^{2+} binding to EF-1, as seen in the crystal structures of recoverin (20), neurocalcin (21), and frequenin (22). To determine whether this structural prediction is correct and to assess how many Ca^{2+} ions bind to DREAM, direct measurements of Ca^{2+} binding were performed.

Equilibrium measurements of $^{45}Ca^{2+}$ binding were conducted on DREAM (Fig. 2). At saturation, three Ca^{2+} ions bind to the protein, consistent with the view that EF-1 is disabled, whereas EF-2, EF-3, and EF-4 are functional. These three functional binding sites are also consistent with previous mutagenesis studies (9, 15). The fractional saturation (Y), which can be obtained from the data, can be represented by the Hill equation:

$$Y = \frac{(Ca^{2+})^a}{(Ca^{2+})^a + K_d^a} \qquad \text{(Eq. 3)}$$

where (Ca^{2+}) is the free Ca^{2+} concentration, K_d is the apparent dissociation constant, and a denotes the Hill coefficient. From the analysis of the Ca^{2+} binding data (Fig. 2), DREAM binds three Ca^{2+} ions with a dissociation constant of 14 μM and a Hill coefficient value of 0.7. The Hill slope (<1.0) and multiphasic Scatchard plot (data not shown) suggest heterogeneous binding of Ca^{2+} and that the three binding sites may have markedly different intrinsic affinities. If the three sites are independent, then the fractional saturation expression simplifies to

$$Y = \frac{(Ca^{2+})}{(Ca^{2+}) + K_{EF2}} + \frac{(Ca^{2+})}{(Ca^{2+}) + K_{EF3}} + \frac{(Ca^{2+})}{(Ca^{2+}) + K_{EF4}} \qquad \text{(Eq. 4)}$$

where K_{EF2} represents the dissociation constant for EF-2, and so forth. The binding data for DREAM are well fit by this equation if $K_{EF3} = K_{EF4} = 5$ μM and $K_{EF2} = 50$ μM, assuming that EF-2 represents the site with weaker affinity. EF-2 contains an aspartate residue (Asp-150) instead of the required glutamate at the 12 position of the calcium-binding loop. The substitution of aspartate for glutamate at residue 150 should dramatically weaken the calcium binding affinity of this site (Fig. 1). Likewise, in recoverin and yeast frequenin, EF-2 was shown to bind Ca^{2+} with much lower affinity than EF-3 and EF-4 (17, 23).

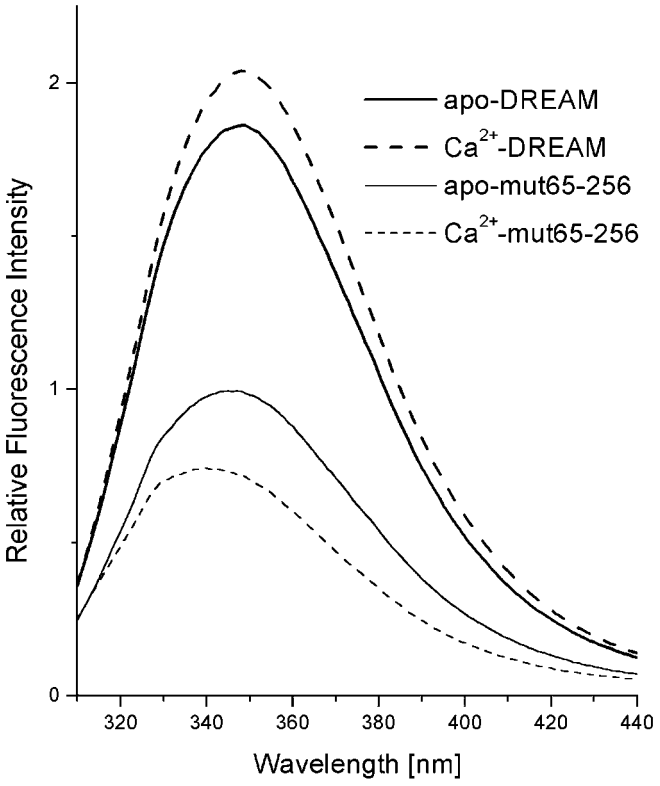

FIG. 3. Fluorescence spectra of DREAM (*bold line*) and mut65–256 (*thin line*). *Solid* and *dashed lines* are used for the apo- and Ca^{2+}-loaded state, respectively. 10 μM DREAM was dissolved in 3 ml of 10 mM Tris-HCl, pH 7.4, 10 mM LDAO, 1 mM DTT, and 1 mM EDTA or 5 mM $CaCl_2$ for the apo- and Ca^{2+}-loaded form, respectively.

Structural Characterization of DREAM—The binding of Ca^{2+} to the EF-hand motifs promotes global structural changes throughout the DREAM protein. As a means to demonstrate the Ca^{2+}-induced structural transitions, we examined the effect of Ca^{2+} on the circular dichroism and intrinsic fluorescence properties of the protein. The far UV CD spectrum of DREAM indicates a typical pattern of α-helical EF-hand proteins containing negative peaks at 222 and 208 nm (data not shown). The negative peaks in the CD spectrum become more pro-

TABLE I

Dynamic light scattering results of DREAM, DREAM · DRE complex, and mut65–256

DLS data were analyzed with a multidispersive model in DynaLS software at a resolution of 1.0. Hydrodynamic radius, R_H, and molecular mass estimated from R_H assuming spherical molecular shape are listed. Molecular masses based on primary sequence are 30 kDa (DREAM), 25 kDa (mut65–256), and 18 kDa (DynDRE and c-*fos* DRE).

	Concentration	R_H (position[a])	Mass (position[a])	R_H (mean[a])	Mass (mean[a])
	μM	*nm*	*kDa*	*nm*	*kDa*
apo-DREAM	17	4.45	108	4.45	108
	33	4.54	114	4.38	104
	67	4.61	118	4.31	100
	130	4.60	117	4.39	115
	200	4.60	117	4.52	112
	270	4.62	118	4.73	125
	330	4.63	120	4.86	134
	430	4.65	120	4.77	128
Ca^{2+}-DREAM	17	3.60	64.7	3.95	81.0
	33	3.67	67.8	3.97	82.0
	67	3.70	69.1	3.75	71.4
	130	3.68	68.2	3.85	76.1
	150	3.75	71.4	4.15	91.3
	180	4.72	125	4.50	111
	200	4.65	120	4.34	102
	270	4.65	120	4.65	120
	330	4.69	123	4.89	136
	430	4.68	122	4.89	136
DREAM/DynDRE[b]	133	5.74	201	6.02	225
DREAM/c-*fos* DRE[b]	150	5.76	202	5.77	203
apo-mut65–256	87	3.82	74.7	4.23	95.6
Ca^{2+}-mut65–256	87	3.12	45.7	3.13	46.1

[a] Peak position and the mean value of the R_H distribution.
[b] Stoichiometry of DREAM and DNA is 1:1.

nounced upon the addition of Ca^{2+}, suggesting that Ca^{2+} binding causes a slight increase in the helical content of DREAM and rearrangement of preexisting EF-hand helices relative to each other, similar to that found in other known EF-hand proteins (24).

The intrinsic tryptophan fluorescence spectra of full-length DREAM and an N-terminal deletion mutant of mouse DREAM (residues 65–256, mut65–256) are presented in Fig. 3. The full-length DREAM protein contains three tryptophan residues (Trp-32, Trp-50, and Trp-169), whereas mut65–256 has only Trp-169. The fluorescence emission of tryptophan in these spectra is very sensitive to its surrounding chemical environment and hence provides an effective probe of structural changes in the protein (25).

The fluorescence emission spectrum of mut65–256 in the absence of Ca^{2+} exhibits an emission maximum at 345 nm, which is shifted to 340 nm upon the addition of saturating amounts of Ca^{2+}. This blue shift in the spectrum indicates a Ca^{2+}-induced structural change in the protein that causes Trp-169 to reside in a more hydrophobic environment in the Ca^{2+}-bound protein.

The fluorescence spectrum of the full-length protein exhibits an emission intensity maximum at 347 nm in the absence of Ca^{2+}, whereas the emission maximum is shifted less than 2 nm upon Ca^{2+} binding to DREAM. These spectra represent the average emission from three tryptophan residues (Trp-32, Trp-50, and Trp-169). Taking into account the Ca^{2+}-induced blue shift of Trp-169 (Fig. 3), the emission from Trp-32 and/or Trp-50 must therefore undergo a Ca^{2+}-induced red shift, suggesting that Trp-32 and/or Trp-50 may occupy a more polar environment in the Ca^{2+}-bound state. Thus, Ca^{2+} binding may promote an allosteric structural change in the N-terminal region that may increase the solvent accessibility of Trp-32 and/or Trp-50. This change in solvent accessibility may be explained in part by the Ca^{2+}-induced change in oligomerization state of DREAM as described below.

Oligomerization of DREAM—Initial DLS studies performed on DREAM (in the absence of detergent) indicated a very broad distribution of hydrodynamic radii, suggesting that the protein solution was polydisperse due to the formation of heterogeneously aggregated species. An extensive screening of various solvent conditions (pH, ionic strength, and detergent) was performed using 50–100 μM DREAM. The addition of detergent (10 mM LDAO) with low salt concentration (<20 mM KCl) at pH 7–8 resulted in a protein solution with a monomodal distribution of the molecular mass of DREAM without any aggregation. These conditions were subsequently used throughout this study.

DLS experiments performed at a variety of protein concentrations were carried out on both apo-DREAM and Ca^{2+}-DREAM. Because the DLS data included light scattering contributions from both protein and the LDAO micelles, a multidispersive model was applied in DynaLS software to fit the observed DLS data at a resolution of 1.0. This analysis enabled the light scattering contribution from the DREAM protein (hydrodynamic radius of 4–5 nm) to be completely resolved from the scattering that corresponded to the LDAO micelle size (hydrodynamic radius of 2.0 nm). Hence, the multidispersive analysis enabled us to accurately extract the size of the protein in the presence of detergent.

Table I summarizes our analysis of the DLS data. The hydrodynamic radius (R_H) of apo-DREAM was measured to be 4.45–4.65 nm at protein concentrations of 17–450 μM. The molecular mass of apo-DREAM was then calculated based on R_H to be 108–120 kDa, assuming a spherical molecular shape. The R_H value of Ca^{2+}-DREAM was 3.60 nm at dilute protein concentrations and increased to 4.65–4.72 nm at protein concentrations greater than 200 μM. The molecular mass of Ca^{2+}-DREAM was calculated from R_H to be 64.7 kDa at dilute protein concentrations (17–150 μM) and 120 kDa at protein concentrations greater than 200 μM. These molecular mass determinations and their protein concentration dependence indicate that apo-DREAM exists as a tetramer, whereas Ca^{2+}-DREAM is a dimer at protein concentrations less than 150 μM and forms a tetramer at protein concentrations higher than 200 μM.

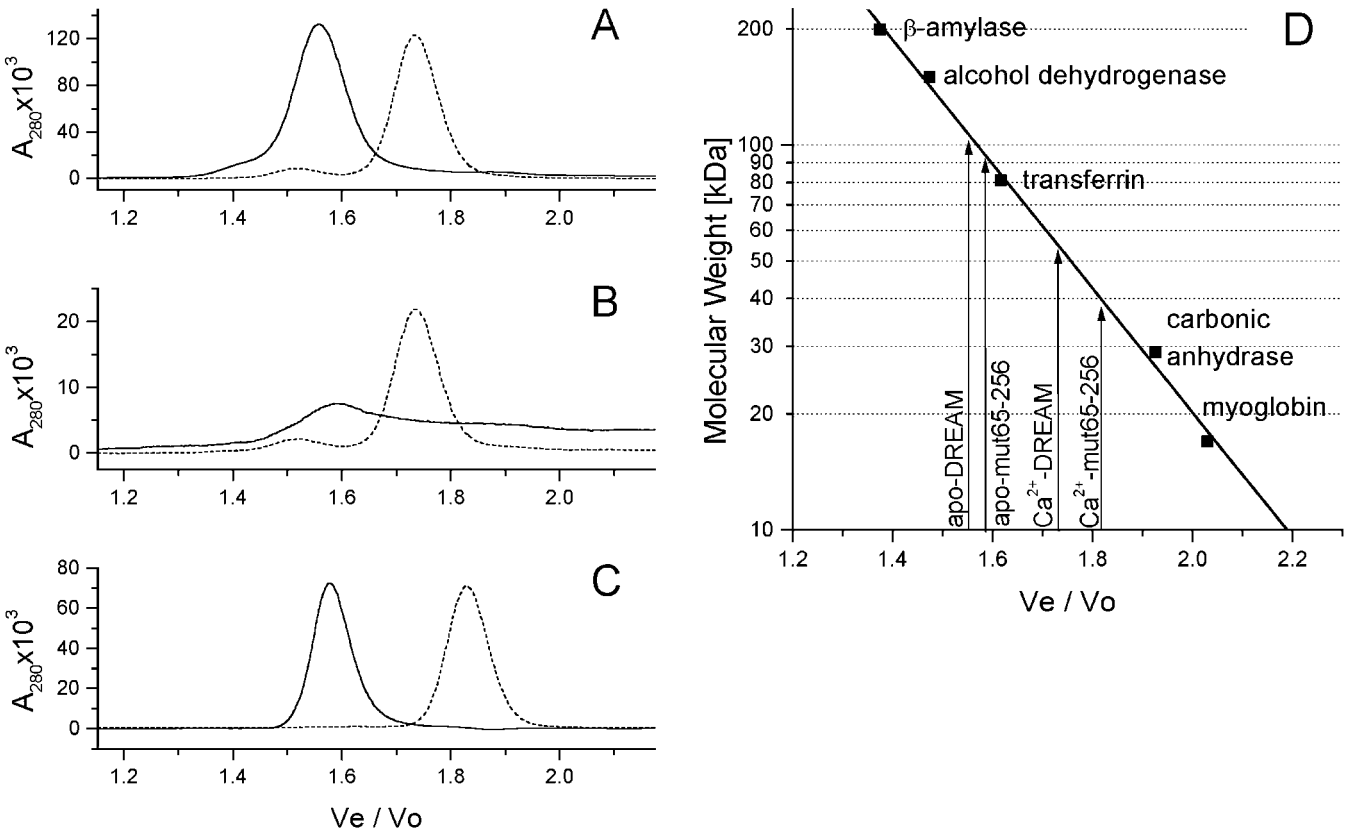

FIG. 4. **Size exclusion chromatograms of apo (*solid line*) and Ca^{2+}-DREAM (*dotted line*).** 100 μl of (*A*) 87 μM and (*B*) 8.7 μM protein solution was applied onto a Superdex 200 HR (10/30) column (Amersham Pharmacia Biotech) pre-equilibrated with the buffers containing 20 mM Tris-HCl pH 7.4, 10 mM LDAO, 1 mM DTT, and 1 mM EDTA or 5 mM $CaCl_2$ for apo-DREAM and Ca^{2+}-DREAM, respectively. *C,* 87 μM apo- (*solid line*) and Ca^{2+}-bound mut65–256 (*dotted line*) was applied under the same conditions. *D,* the standard curve for the molecular mass determination was created using β-amylase (200 kDa), alcohol dehydrogenase (150 kDa), transferrin (81 kDa), carbonic anhydrase (29 kDa), and myoglobin (17 kDa). Void volume of the column (V_0) was obtained as 7.82 ml using blue dextran (2000 kDa), and V_e is a volume of elution of each sample. *Arrows* stand for V_e/V_0 values for in the apo- or Ca^{2+}-loaded form of 87 μM DREAM and mut65–256. Molecular masses based on amino acid sequence are 30 and 25 kDa for DREAM and mut65–256, respectively.

The molecular mass of DREAM was also confirmed by size exclusion chromatography. The apo-DREAM at an initial concentration of 87 μM eluted in a single peak with a relative elution volume $V_e/V_0 = 1.55$ (Fig. 4*A*), calibrated to a molecular mass of 107 kDa (Fig. 4*D*). In contrast, the Ca^{2+}-bound protein exhibited a much longer elution time ($V_e/V_0 = 1.73$), calibrated to a molecular mass of 55 kDa (Fig. 4*D*). At a more dilute protein concentration (8.7 μM), apo-DREAM showed a very broad elution pattern (Fig. 4*B*). A partially resolved peak ($V_e/V_0 = 1.58$) representing the tetramer species was flanked by shoulder peaks corresponding to dimer and monomer species. In contrast, the dilute Ca^{2+}-DREAM eluted in a single peak corresponding to dimer ($V_e/V_0 = 1.73$ and molecular mass = 55 kDa).

Similar Ca^{2+}-induced changes in molecular mass and oligomerization state were also observed for a C-terminal fragment of mouse DREAM (residues 65–256, mut 65–256) containing only the four EF-hand Ca^{2+}-binding sites. The DLS analysis indicated that apo-mut65–256 forms a tetramer (R_H = 4.23 nm; molecular mass = 95.6 kDa), whereas Ca^{2+}-bound mut65–256 forms a dimer (R_H = 3.13 nm; molecular mass = 46.1 kDa). In addition, the size exclusion chromatography results on mut65–256 are consistent with the DLS analysis and indicate that mut65–256 forms a tetramer ($V_e/V_0 = 1.58$; molecular mass = 94 kDa) and dimer ($V_e/V_0 = 1.82$; molecular mass = 39 kDa) in the apo- and Ca^{2+}-loaded states, respectively (Fig. 4*C*). Therefore, the C-terminal Ca^{2+}-binding region must be responsible for the oligomerization of DREAM.

In summary, apo-DREAM has a propensity to form a tetramer at protein concentrations higher than 20 μM. The Ca^{2+}-bound DREAM forms a stable dimer at low protein concentrations and forms a tetramer at concentrations higher than 200 μM. The dramatically different hydrodynamic properties observed here for the Ca^{2+}-free and Ca^{2+}-bound forms of DREAM may also be due, in part, to possible Ca^{2+}-induced changes in molecular shape. However, the sharp dependence of the DLS and size exclusion chromatography data on protein concentration (Table I and Fig. 4*B*) indicates that the observed hydrodynamic changes of the protein are also the result of protein oligomerization. Very similar Ca^{2+}-dependent oligomerization properties were observed for the C-terminal fragment, mut65–256. Hence, Ca^{2+}-induced structural changes in the C-terminal EF-hand region may be crucial for the alteration of its oligomerization state. Other recoverin-like proteins are also known to exhibit Ca^{2+}-regulated dimerization. For example, neurocalcin forms a dimer in the Ca^{2+}-bound state (21), whereas Ca^{2+}-free neurocalcin is monomeric (26). Conversely, guanylate cyclase-activating protein-2 forms a dimer only in the Ca^{2+}-free state and is monomeric in the Ca^{2+}-bound state (26).

DNA Binding Studies—DREAM was reported to suppress the expression of human prodynorphin and c-*fos* genes by binding to their DRE (9). The c-*fos* DRE sequence has high similarity to the reverse sequence of DynDRE, and EMSA previously showed that three DREs of DynDRE, c-*fos* DRE, and reversed DynDRE have comparable affinity to apo-DREAM (9, 15). We applied ITC to quantitatively investigate the energetics of DREAM binding to the duplexes of DNA oligonucleotides corresponding to the DRE sequence of prodynorphin and c-*fos*. All

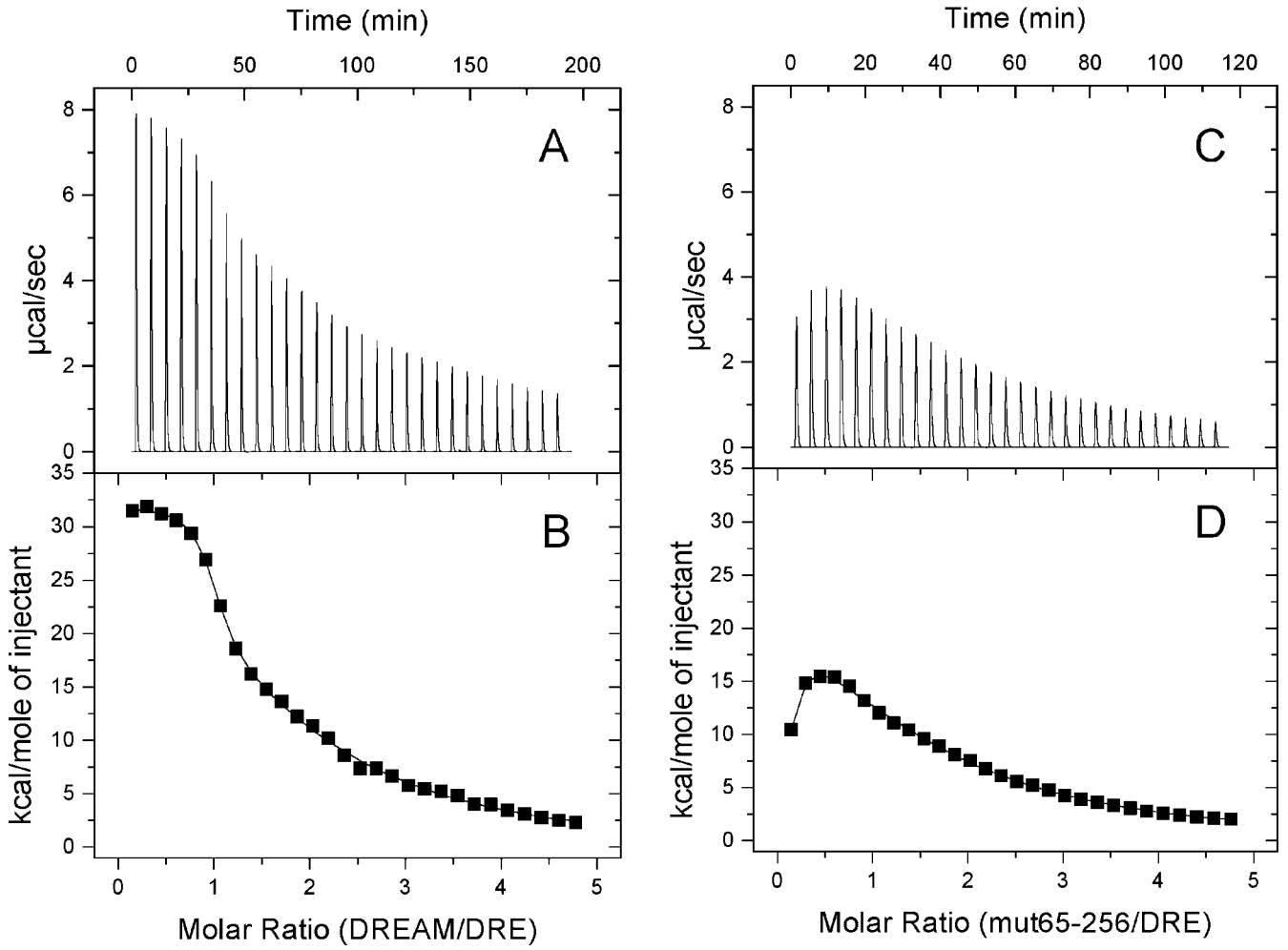

FIG. 5. **Isothermal titration microcalorimetric analyses of the DREAM-DRE interaction.** *A,* trace of the calorimetric titration of 29 × 10 μl aliquots of apo-DREAM into the cell containing DynDRE DNA. *B,* integrated binding isotherm obtained from the experiment shown in *A* and experimental fit to a two-site model. *C,* trace of the calorimetric titration of 29 × 10 μl aliquots of apo-mut65–256 into the cell containing DynDRE DNA. *D,* integrated binding isotherm obtained from the experiment shown in *C* and experimental fit to a two-site model. Binding parameters yielded by the best fit (*solid line*) are listed in Table II.

ITC experiments were carried out using 10 mM LDAO detergent and a salt concentration less than 10 mM. These solvent conditions were necessary to achieve reproducible detection of heat exchange in the titration.

The apo-DREAM protein exhibited endothermic binding to DynDRE, as indicated by a relatively large and positive enthalpy of binding (+25 kcal/mol) observed in the calorimetric titration (Fig. 5, *A* and *B*). In contrast, very little enthalpy (<4 kcal/mol) was observed in the titration of Ca^{2+}-DREAM with DynDRE (data not shown). Thus, apo-DREAM is the more active form of the protein that binds to DynDRE, and Ca^{2+}-DREAM does not exhibit any appreciable binding. The positive heat of formation of the apo-DREAM·DRE complex (Fig. 5, *A* and *B*) indicates that this interaction is an enthalpically unfavorable (entropically driven) process that may include desolvation of water molecules and/or conformational changes induced by DRE binding. Other DNA-binding proteins such as the TATA-binding protein (27), nuclear hormone receptors (28), and the Cro repressor (29) also exhibit similar entropically dominated binding to DNA.

The stoichiometry of DRE binding was also determined from our analysis of the calorimetry data. Analysis using a one-site model indicated that one molecule of DRE was bound to each DREAM polypeptide. Because apo-DREAM forms a tetramer as described above, the observed stoichiometry of 1 indicates that each DREAM tetramer contains four DNA binding sites. The complexation of a DREAM tetramer with four molecules of DNA was also confirmed by DLS, which gave a molecular mass of 200–230 kDa corresponding to a DREAM tetramer (120 kDa) bound to four molecules of DRE (18 kDa × 4) (Table I).

To minimize protein aggregation and more accurately dissect DRE binding energetics, a reverse calorimetric titration was performed in which aliquots of apo-DREAM in the syringe were sequentially injected into the sample cell containing DynDRE (Fig. 5*A*). The observed isotherm in this case is multiphasic and must be deconvoluted using a model with multiple binding sites (Fig. 5*B*). The ITC data for the reverse titration were best fit using a two-site model whose thermodynamic parameters are listed in Table II. The first site in this model has a much higher affinity ($K_1 = 1.3 \times 10^7$ M^{-1}) and larger enthalpy ($n_1 \times \Delta H_1^0 = 24$ kcal/mol) than those of the other site ($K_2 = 1.6 \times 10^6$ M^{-1} and $n_2 \times \Delta H_2^0 = 0.8$ kcal/mol). The stoichiometry of the high and low affinity sites are 0.25 and 0.75 mole protein/mole DRE, respectively. A plausible interpretation would be that a preformed apo-DREAM tetramer binds one DNA molecule with markedly higher affinity than that of the other three molecules of DNA. The electrostatic repulsion created by the binding of multiple DNA molecules to one DREAM tetramer might explain the apparent anticooperativity of DNA binding, giving rise to the high and low affinity sites. The single high affinity site on an apo-DREAM tetramer is likely to be biologically more relevant because the DREAM tetramer concentration should

TABLE II
Thermodynamic parameters for binding of DRE and apo-DREAM/mut65–256

The best fit to the ITC data was obtained by applying a two-site model where n_i, K_i, and ΔH_i^0 are the number of DREs per DREAM, the association constant, and the standard enthalpy change at the ith binding site on the protein.

Protein	DNA	n_1	$K_1 \times 10^{-6}$	ΔH_1^0	n_2	$K_2 \times 10^{-6}$	ΔH_2^0
			(M^{-1})	$(kcal/mol^{-1})$		(M^{-1})	$(kcal/mol^{-1})$
DREAM	DynDRE	0.264 ± 0.001	13 ± 2	90 ± 6	0.80 ± 0.03	1.6 ± 0.3	1.0 ± 0.1
DREAM	c-*fos* DRE	0.23 ± 0.02	4 ± 1	80 ± 18	0.79 ± 0.07	0.7 ± 0.2	8.5 ± 4.5
mut65–256	DynDRE	0.263 ± 0.006	5 ± 3	76 ± 3	3.5 ± 0.3	0.18 ± 0.09	−2.4 ± 0.3

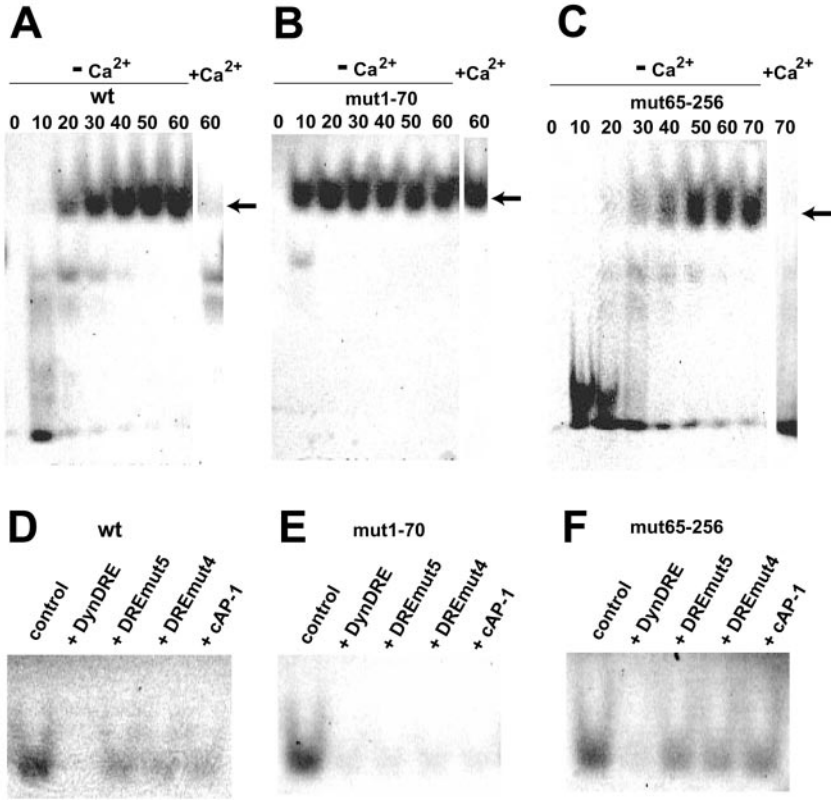

FIG. 6. **Fluorescent EMSA of mDREAM-DRE interaction.** *A,* EMSA titration of full-length mDREAM (0–60 μM) into Cy5-labeled DRE (5 nM) in the presence and absence of 10 mM Ca^{2+}. The shifted band, corresponding to the ones seen in $-Ca^{2+}$ (*arrow*), was not detected in the presence of Ca^{2+}; therefore, only the 60 μM lane is shown. *B,* EMSA titration of the N-terminal fragment (mut1–70) of mDREAM (0–60 μM) into Cy5-labeled DRE (5 nM) in the presence and absence of 10 mM Ca^{2+}. The shifted band, corresponding to the ones seen in $-Ca^{2+}$ (*arrow*), was also detected in the presence of Ca^{2+} (only the 60 μM lane is shown). *C,* EMSA titration of the C-terminal fragment (mut65–256) of mDREAM (0–70 μM) into Cy5-labeled DRE (5 nM) in the presence and absence of 10 mM Ca^{2+}. The shifted band, corresponding to the ones seen in $-Ca^{2+}$ (*arrow*), was not detected in the presence of Ca^{2+} (only the 70 μM lane is shown). For competition EMSA, (*D*) 40 μM wild type mDREAM, (*E*) 10 μM purified mut1–70, and (*F*) 80 μM purified mut65–256 were incubated with 5 nM Cy5-labeled DynDRE. (*D*) 75 nM (15-fold excess), (*E*) 325 nM (65-fold excess), and (*F*) 75 nM (15-fold excess) of unlabeled DynDRE, DREmut5, DREmut4, or cAP-1 were added to the same sample as the control lane, respectively.

be much higher than that of DRE in the cell nucleus. Under these conditions, the DRE binding would be limited primarily to the high affinity site on the DREAM tetramer.

The binding of c-*fos* DRE to apo-DREAM and the energetics of this interaction were found to be very similar to what we had measured for the DynDRE interaction (Fig. 5, *A* and *B*; Table II). The binding isotherm (data not shown) was biphasic and fit using a two-site model (Table II). The affinity of the first site for c-*fos* DRE ($K_1 = 4 \times 10^6$ M^{-1}) is slightly lower than that of DynDRE. The other binding parameters for c-*fos* DRE are nearly identical to those of DynDRE. The three-dimensional structures of the protein·DNA complexes are needed to understand how apo-DREAM recognizes these different DNA sequences.

Localization of the DNA Binding Site—To attempt to localize the DNA-binding region in DREAM, we made a series of deletion mutants of mouse DREAM (91% identical to human calsenilin/DREAM, see Fig. 1), which are defined as mut1–70 (residues 1–70), mut1–96 (residues 1–96), and mut65–256 (residues 65–256). These protein fragments were tested for their ability to bind the DRE using EMSA (Fig. 6) and ITC. Only the Ca^{2+}-free forms of the full-length protein and mut65–256 show sequence-specific binding to DynDRE, whereas the Ca^{2+}-bound forms do not exhibit any detectable binding. Interestingly, mut1–70 and mut1–96 appear to bind to DynDRE regardless of Ca^{2+} and do not exhibit sequence specificity (Fig. 6, *B* and *E*). Thus, the DNA-binding region appears to include residues from both the N-terminal basic and C-terminal Ca^{2+}-binding regions.

ITC studies were carried out on the deletion mutants to quantify and evaluate the energetics of DNA binding to the N-terminal (mut1–96) and C-terminal Ca^{2+}-binding (mut65–256) regions (note that mut1–70 protein could not be obtained in high enough quantities to be studied by ITC). Titration of mut1–96 to DRE yielded a detectable amount of heat exchange (~4–5 kcal/mol) regardless of the Ca^{2+} concentration, indicating that the mut1–96 protein binds to DRE (data not shown). The amount of heat exchange here is quite small and is comparable to the very slight enthalpy of DRE binding observed for the Ca^{2+}-bound full-length DREAM (data not shown). Thus, the very weak DRE binding to Ca^{2+}-bound DREAM detected by ITC may be due to an exposed N-terminal basic region that weakly binds the DRE.

The ITC isotherm of apo-mut65–256 titration into DynDRE is shown in Fig. 5, *C* and *D*, and the thermodynamic parameters are summarized in Table II. The biphasic nature of the isotherm suggests two binding sites with markedly different affinities. The first binding site of mut65–256 exhibits a dissociation constant (K_{d1} = 200 nM) and enthalpy ($n_1 \times \Delta H_1^0$ = 20 kcal/mol) that are similar to those of the full-length protein. The second site of mut65–256 exhibits much weaker affinity (K_{d2} = 5 μM) with a negative enthalpy change. The negative enthalpy for the low affinity site of mut65–256 explains, in part, why the total enthalpy of the full-length protein ($n_1 \times$

$\Delta H_1^0 + n_2 \times \Delta H_2^0$ = 25 kcal/mol) is larger than that of mut65–256 (12 kcal/mol). The lower total enthalpy for mut65–256 could also be explained by a lack of enthalpy contributed from the N-terminal basic region (residues 1–65), which is further evidence that the N-terminal region does indeed contribute to DRE binding. Correspondingly, the full-length protein binds DRE with 2-fold higher apparent affinity compared with that of mut65–256.

Although the N-terminal region does contribute to the energetics of DRE binding, the biological significance of the N-terminal region remains uncertain. The thermodynamics of DRE binding to the functional, high affinity site of mut65–256 is very similar to that of the full-length protein (Table II). Also, like the full-length protein, mut65–256 forms a tetramer in the Ca^{2+}-free state that dissociates into dimers in the Ca^{2+}-bound state. Hence, it would seem that mut65–256 possesses all the essential features to serve as a Ca^{2+}-regulated transcriptional repressor. Consistent with this view is the recent report that DREAM has a caspase-3 cleavage site at residues Asp-61-Asp-64 located between the N-terminal basic region and the C-terminal Ca^{2+}-binding region (12). The data obtained here suggest that DREAM may function as a transcriptional repressor even after cleavage by caspase-3.

Mechanism of Ca^{2+}-regulated DNA Binding to DREAM—In this study, we demonstrate that Ca^{2+}-free DREAM forms a tetramer in the protein·DNA complex, whereas the Ca^{2+}-bound protein forms a dimer under physiological conditions and does not bind appreciably to DNA. The N-terminal region (mut1–70 and mut1–96) contributes somewhat to the energetics of DNA binding, and the C-terminal region (mut65–256) exhibits Ca^{2+}-regulated oligomerization and DNA binding akin to that of the full-length protein. As a result, the DNA-binding site may consist of contacts made by residues from both the N-terminal and C-terminal regions. However, the N-terminal region does not appear to be essential for the Ca^{2+}-regulated oligomerization. In addition, we measured a binding stoichiometry of four DNA molecules bound to one DREAM tetramer. These results suggest two possible modes of Ca^{2+}-regulated DNA binding. Each polypeptide subunit of the tetramer could contain an individual DNA-binding site that may be altered by Ca^{2+}-induced structural changes within each subunit. Alternatively, the DNA-binding sites could be integrally generated by tetramer formation, in which case the sites might be disassembled by Ca^{2+}-induced dissociation of the tetramer. The observed anticooperativity of DNA binding suggests that the four DNA-binding sites are coupled and might be spatially close to one another. Clearly, the three-dimensional atomic resolution structure of the DREAM tetramer bound to DNA will need to be determined to more fully understand the precise mechanism of Ca^{2+}-regulated DNA binding.

Conclusion—The recombinant form of calsenilin/DREAM/KChIP3 was expressed, purified, and characterized using several physicochemical methods. Our light scattering and calorimetry studies reveal that a preformed tetramer of apo-DREAM binds four molecules of DRE. The binding of three Ca^{2+} ions to each DREAM polypeptide subunit causes the tetrameric protein to dissociate into dimers and may disrupt the Ca^{2+}-bound protein from binding to DNA. One DRE molecule binds to an apo-DREAM tetramer with high affinity (K_d = 75 nM), and the other three DRE molecules bind with markedly lower affinity (K_d = 700 nM), presumably due to anticooperativity. We suggest that the single site with highest affinity may be biologically most important because the DREAM tetramer concentration in the cell nucleus is likely to be much higher than the DRE concentration. Hence, there may not be enough DRE molecules in the cell nucleus to fill the low affinity sites. The tetramer of DREAM bound to only one DNA element may be structurally unique as a transcriptional regulator complex.

Our results suggest that the DNA-binding sites on DREAM appear delocalized and may consist of residues from both the N-terminal and C-terminal regions. Therefore, we suggest that Ca^{2+}-induced structural changes within the EF-hand motifs observed in this study lead to the dissociation of the tetrameric protein into dimers, which in turn may alter the DNA-binding sites. Our next goal is to further elucidate and more rigorously analyze the Ca^{2+}-regulated DNA binding by DREAM by determining the atomic resolution three-dimensional structure of the protein·DNA complex.

Acknowledgments—We thank F. Schwarz for assistance with the ITC experiments and F. Song for DNA synthesis.

REFERENCES

1. Berridge, M. J. (1997) *J. Physiol.* **499,** 291–306
2. Ikura, M. (1996) *Trends Biochem. Sci.* **21,** 14–17
3. Moncrief, N. D., Kretsinger, R. H., and Goodman, M. (1990) *J. Mol. Evol.* **30,** 522–562
4. Dizhoor, A. M., Ray, S., Kumar, S., Niemi, G., Spencer, M., Brolley, D., Walsh, K. A., Philipov, P. P., Hurley, J. B., and Stryer, L. (1991) *Science* **251,** 915–918
5. Takamatsu, K., Kitamura, K., and Noguchi, T. (1992) *Biochem. Biophys. Res. Commun.* **183,** 245–251
6. Pongs, O., Lindemeier, J., Zhu, X. R., Theil, T., Engelkamp, D., Krah-Jentgens, I., Lambrecht, H. G., Kock, K. W., Schwerner, J., Rivosecchi, R., Mallart, A., Galceran, J., Canal, I., Barbas, J. A., and Ferrus, A. (1993) *Neuron* **11,** 15–28
7. Ames, J. B., Tanaka, T., Stryer, L., and Ikura, M. (1996) *Curr. Opin. Struct. Biol.* **6,** 432–438
8. Buxbaum, J. D., Choi, E. K., Luo, Y., Lilliehook, C., Crowley, A. C., Merriam, D. E., and Wasco, W. (1998) *Nat. Med.* **4,** 1177–1181
9. Carrion, A. M., Link, W. A., Ledo, F., Mellstrom, B., and Naranjo, J. R. (1999) *Nature* **398,** 80–84
10. An, W. F., Bowlby, M. R., Betty, M., Cao, J., Ling, H. P., Mendoza, G., Hinson, J. W., Mattsson, K. I., Strassle, B. W., Trimmer, J. S., and Rhodes, K. J. (2000) *Nature* **403,** 553–556
11. Leissring, M. A., Yamasaki, T. R., Wasco, W., Buxbaum, J. D., Parker, I., and LaFerla, F. M. (2000) *Proc. Natl. Acad. Sci. U. S. A.* **97,** 8590–8593
12. Choi, E. K., Zaidi, N. F., Miller, J. S., Crowley, A. C., Merriam, D. M., Lilliehook, C., Buxbaum, J. D., and Wasco, W. (2001) *J. Biol. Chem.* **276,** 19197–19204
13. Sanz, C., Mellstrom, B., Link, W. A., Naranjo, J. R., and Fernandez-Luna, J. L. (2001) *EMBO J.* **20,** 2286–2292
14. Ledo, F., Carrion, A. M., Link, W. A., Mellstrom, B., and Naranjo, J. R. (2000) *Mol. Cell. Biol.* **20,** 9120–9126
15. Ledo, F., Link, W. A., Carrion, A. M., Echeverria, V., Mellstrom, B., and Naranjo, J. R. (2000) *Biochim. Biophys. Acta* **1498,** 162–168
16. Carrion, A. M., Mellstrom, B., and Naranjo, J. R. (1998) *Mol. Cell. Biol.* **18,** 6921–6929
17. Ames, J. B., Hendricks, K. B., Strahl, T., Huttner, I. G., Hamasaki, N., and Thorner, J. (2000) *Biochemistry* **39,** 12149–12161
18. Moradian-Oldak, J., Leung, W., and Fincham, A. G. (1998) *J. Struct. Biol.* **122,** 320–327
19. Wiseman, T., Williston, S., Brandts, J. F., and Lin, L. N. (1989) *Anal. Biochem.* **179,** 131–137
20. Flaherty, K. M., Zozulya, S., Stryer, L., and McKay, D. B. (1993) *Cell* **75,** 709–716
21. Vijay-Kumar, S., and Kumar, V. D. (1999) *Nat. Struct. Biol.* **6,** 80–88
22. Bourne, Y., Dannenberg, J., Pollmann, V. V., Marchot, P., and Pongs, O. (2001) *J. Biol. Chem.* **276,** 11949–11955
23. Ames, J. B., Porumb, T., Tanaka, T., Ikura, M., and Stryer, L. (1995) *J. Biol. Chem.* **270,** 4526–4533
24. Yap, K. L., Ames, J. B., Swindells, M. B., and Ikura, M. (1999) *Proteins* **37,** 499–507
25. Freifelder, D. (1982) in *Physical Biochemistry: Applications to Biochemistry and Molecular Biology*, 2nd Ed., pp. 537–572, W. H. Freeman and Company, San Francisco, CA
26. Olshevskaya, E. V., Ermilov, A. N., and Dizhoor, A. M. (1999) *J. Biol. Chem.* **274,** 25583–25587
27. O'Brien, R. O., DeDecker, B., Fleming, K. G., Sigler, P. B., and Ladbury, J. E. (1998) *J. Mol. Biol.* **279,** 117–125
28. Lundback, T., and Hard, T. (1996) *Proc. Natl. Acad. Sci. U. S. A.* **93,** 4754–4759
29. Takeda, Y., Ross, P. D., and Mudd, C. P. (1992) *Proc. Natl. Acad. Sci. U. S. A.* **89,** 8180–8184